Numerical advances in Self-Consistent Field Theory simulations of Block Copolymers

Carlos Garcia-Cervera

Mathematics Department, UCSB

IPAM, UCLA, 2013

Collaborators

- Hector D. Ceniceros, Mathematics, UCSB
- Kris Delaney, MRL, UCSB
- Glenn H. Fredrickson, MRL, UCSB
- Edward Kramer, Materials, UCSB

- Su-Mi Hur, Chemical Eng., U. Wisconsin-Madison
- Tanya Chantawansri, Army Research Lab, Maryland
- Sean Paradiso, Chemical Eng., UCSB
- Per Von Soosten, Mathematics, UCSB

Block Copolymer Lithography

- Thermodynamic incompatibility & chemical bonding
  → microscopic phase separation

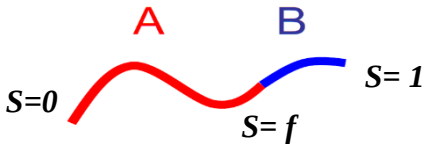

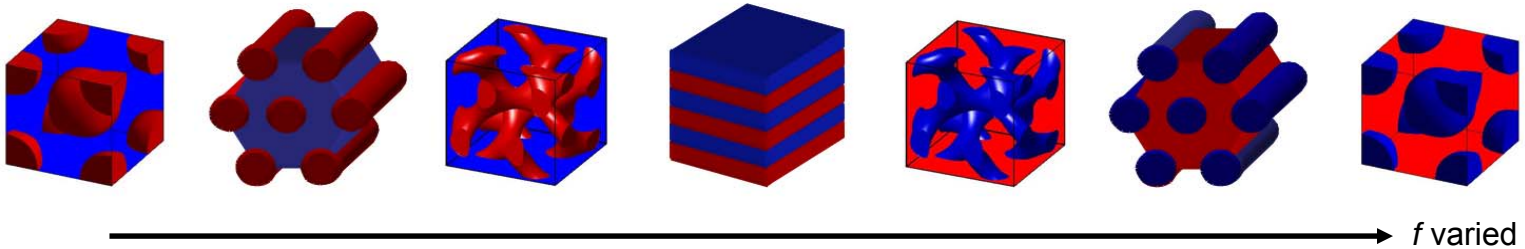

- Self-assembly of block copolymer thin films: a promising high resolution, next generation lithographic tool

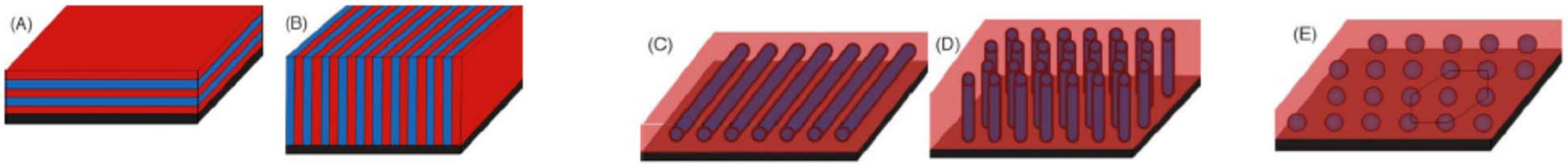

R. Segalman, *Matl. Sci. & Eng.* **2005**, 48, 191-226.

Bulk Phases of Diblock Copolymers

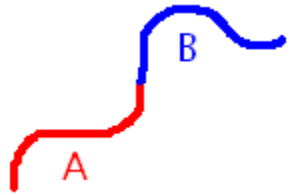

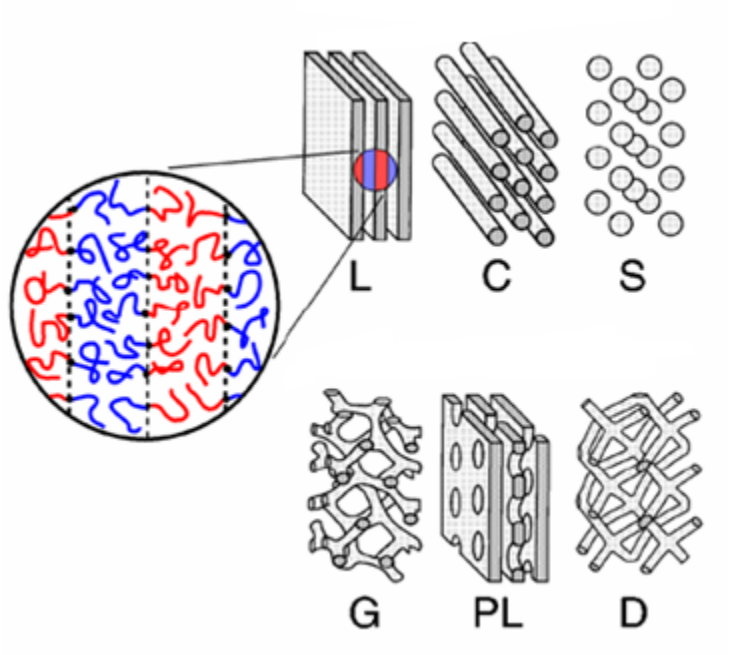

M.W. Matsen, *J.Physics: Condens. Matter*. 2002, 14, R21-R47

- In 3D we can see 6 bulk phases
  - L: Lamellar
  - C: Cylindrical
  - S: Spherical
  - G: Gyroid
  - PL: Perforated-lamellar
  - D: Double Diamond
- In 2D we can only see 2 of these phases
  - L: Lamellar
  - C: Cylindrical

Directed Self-Assembly

- Long range dimensional control – removal of defects and grain boundaries
- Placement accuracy: satisfying alignment and registration tolerances

Chemically Patterned Substrate

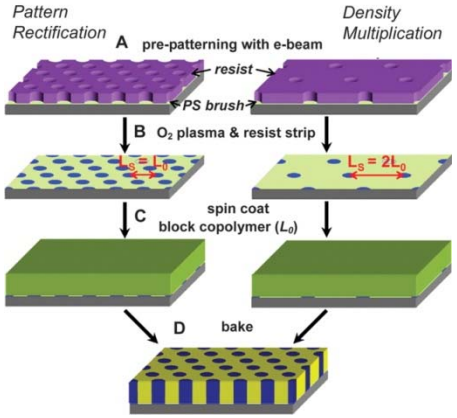

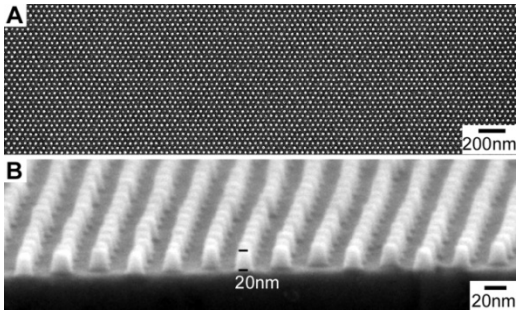

R. Ruiz et al. Science 2008, 321(5891), 936

Topographically Patterned Substrate (graphoepitaxy)

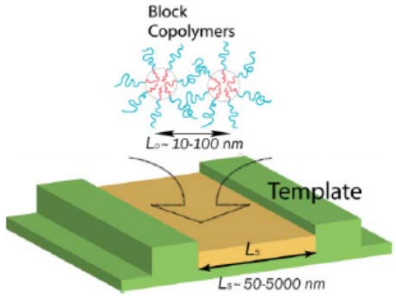

Joy Y. Cheng et al. Adv. Mater. 18, 2505 (2006)

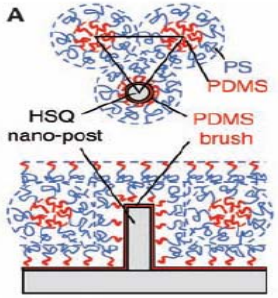

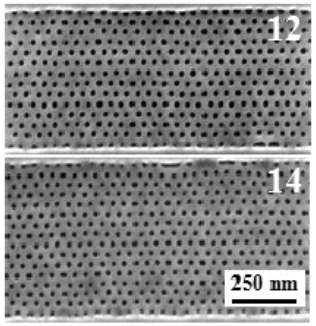

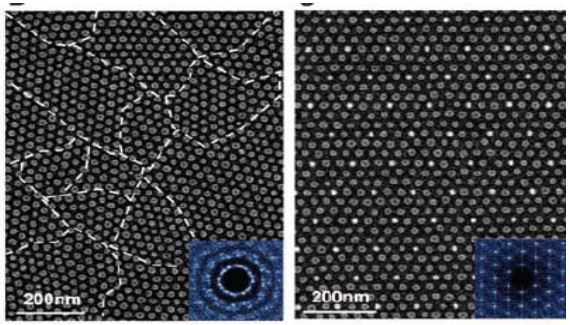

S. Xiao et al. *Nanotechnology,* **16**, S324 (2005)

Ion Bita, et al. *Science* **321**, 939 (2008)

Requirements for Block Copolymer Lithography

- Improved long range dimensional control
- Placement accuracy: satisfying alignment and registration tolerances
- Improved resolution and linear density - beyond the 10 nm?
- Basis set of essential features

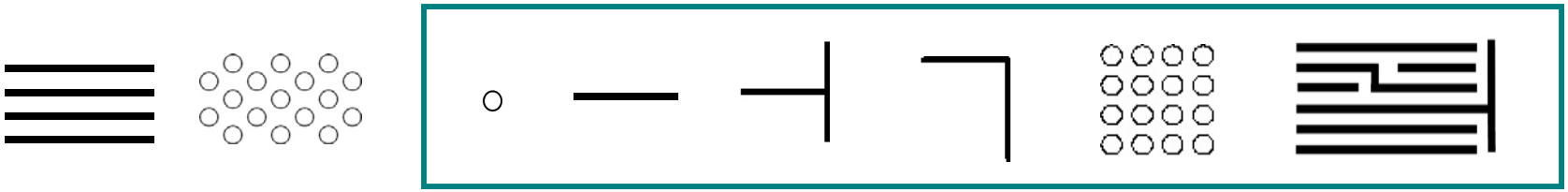

Non-natural structures

- Features with multiple sizes and pitches in the same layer
- Satisfying pattern transfer requirements and integration
- Enhanced process window
- Achieving throughput requirements, either via single wafer or batch processing: average net throughput of ~1 wafer per 1-2 minutes

Evaporation Dynamics

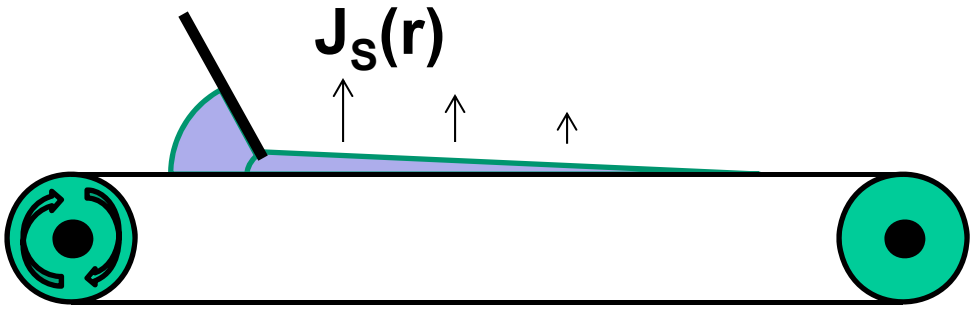

http://www1.eere.energy.gov/solar/sunshot/pv_organic.html

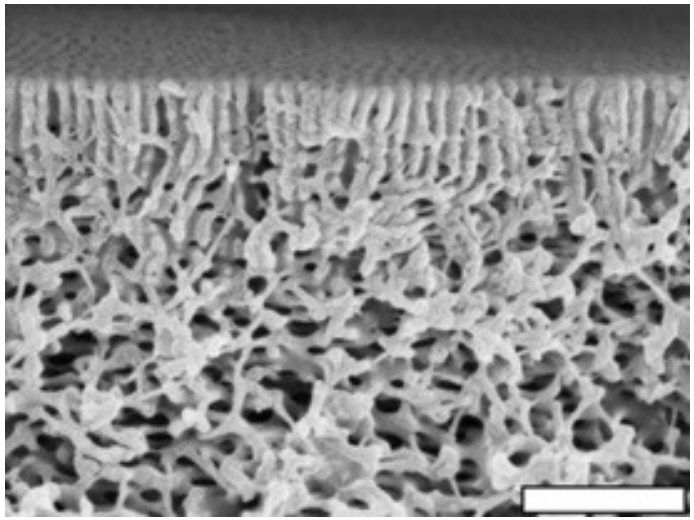

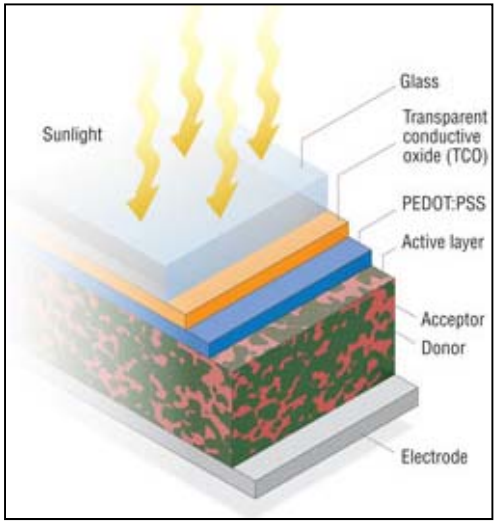

Peinemann, Abetz, Simon, *Nature Materials,* **6,** 992-996 (2007)

Pattern Selection via Controlled Evaporation

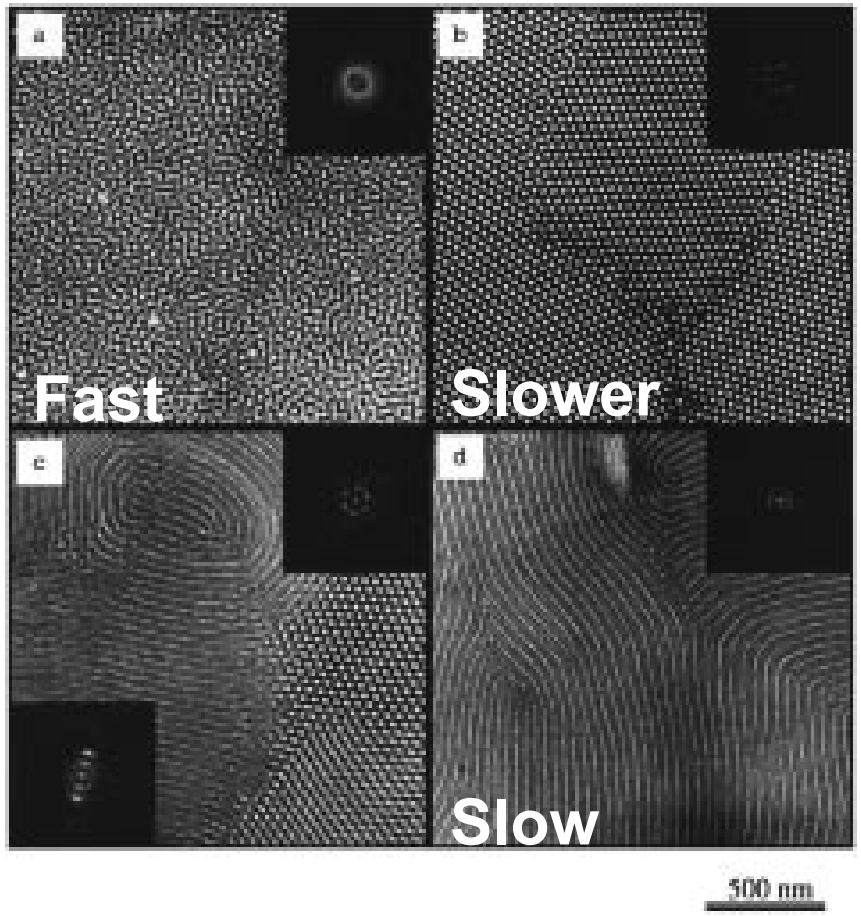

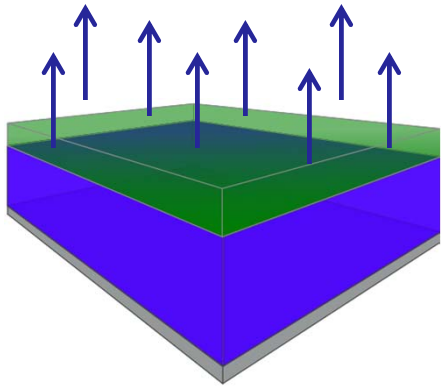

Kim, G., & Libera, M. (1998). Morphological development in solvent-cast polystyrene-polybutadiene-polystyrene (SBS) triblock copolymer thin films. *Macromolecules*, *31*(8), 2569–2577. doi:10.1021/ma971349i

Self-Consistent Field Theory (SCFT)

- Particle based model: many Gaussian chains interacting with each other (~ Wiener Process)

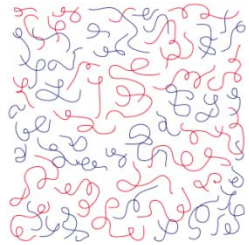

$$Z = \int \mathcal{D}\mathbf{r} \exp(-\beta U[\mathbf{r}]) \qquad U[\mathbf{r}] \text{ : potential energy}$$

Hubbard-Stratonovich Transformation

- Fi $$Z = \int \mathcal{D}w \exp(-H[w]) \qquad H[w] = C \int_V d\mathbf{x}\, h(w) - n \ln Q[w]$$

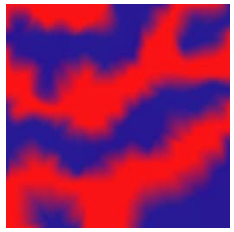

$H[w]$: effective Hamiltonian (energy functional of field w)
C : coordination number (dimensionless chain concentration)
$Q[w]$: a single chain partition function in an external field w

- Mean field approximation: single configuration dominates the partition

$$Z = \int \mathcal{D}w \exp(-H[w]) \xrightarrow{\infty} Z \approx \exp(-H[w^*]) \qquad \beta A = -lnZ \approx H[w^*]$$

Self-Consistent Field Theory

- Single-chain partition function *Q*

$$Q[w] = \frac{1}{V}\int_V E_{\mathbf{x}}\left[\exp\left\{-\int_0^1 w(X_s)\,ds\right\}\right]\,d\mathbf{x}$$

- Energy functional *H* [*w*] and density operators can be evaluated from chain propagator *q* (x, s ; [w]) (Feynman-Kac)

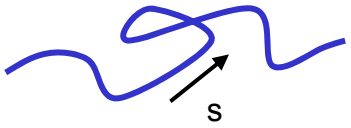

$q(\mathbf{x}, s; [w])$

$$Q[w] = \frac{1}{V}\int_V q(\mathbf{x}, 1)\,d\mathbf{x}$$

$$\begin{aligned}\frac{\partial}{\partial s}q(\mathbf{x}, s; [w]) &= \Delta q(\mathbf{x}, s; [w]) - w(\mathbf{x})q(\mathbf{x}, s; [w]),\\ q(\mathbf{x}, 0; [w]) &= 1, \text{ plus b.c.}\end{aligned}$$

E. Helfand, *J. Chem. Phys.* 62, 999-1005 (1975)

M.W. Matsen, M. Schick, *Phys. Rev. Lett.* 72, 2660-2663 (1994)

SCFT Equations

- Effective Hamiltonian:

$$H[W,\Sigma] = \int_V \left((1-2f)W - \Sigma + \frac{1}{\chi_N} W^2 \right) dx - V \ln Q[W,\Sigma],$$

where

$$Q[W,\Sigma] = \frac{1}{V} \int_V q(x,1)\, dx,$$

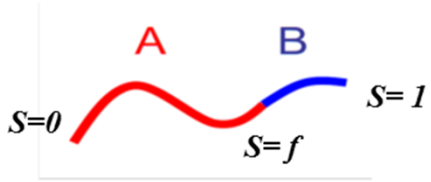

and q satisfies the diffusion equation

$$\begin{aligned} \frac{\partial q}{\partial s} &= \Delta q - \psi q, \quad x \in V, \quad s \in (0,1), \\ q(x,0) &= 1. \end{aligned}$$

We have defined

$$\psi = \begin{cases} \Sigma - W, & 0 \le s \le f, \\ \Sigma + W, & f < s \le 1. \end{cases}$$

SCFT Equations – Gradient Flow

- Dynamics:
  - Mean field (saddle point) solution (SCFT)
  - Solving for Q and densities: most numerically expensive step.

$$
\begin{aligned}
\frac{\partial W}{\partial t} &= \phi_A(x;W,\Sigma) - \phi_B(x;W,\Sigma) + 1 - 2f - \frac{1}{\chi_N} W, \\
\frac{\partial \Sigma}{\partial t} &= \phi_A(x;W,\Sigma) + \phi_B(x;W,\Sigma) - 1, \\
\phi_A(x;W,\Sigma) &= \frac{1}{Q}\int_0^f q(x,s)q^\dagger(x,1-s)\,ds, \\
\phi_B(x;W,\Sigma) &= \frac{1}{Q}\int_f^1 q(x,s)q^\dagger(x,1-s)\,ds, \\
Q &= \frac{1}{V}\int_V q(x,1)\,dx.
\end{aligned}
$$

Basic Schematic

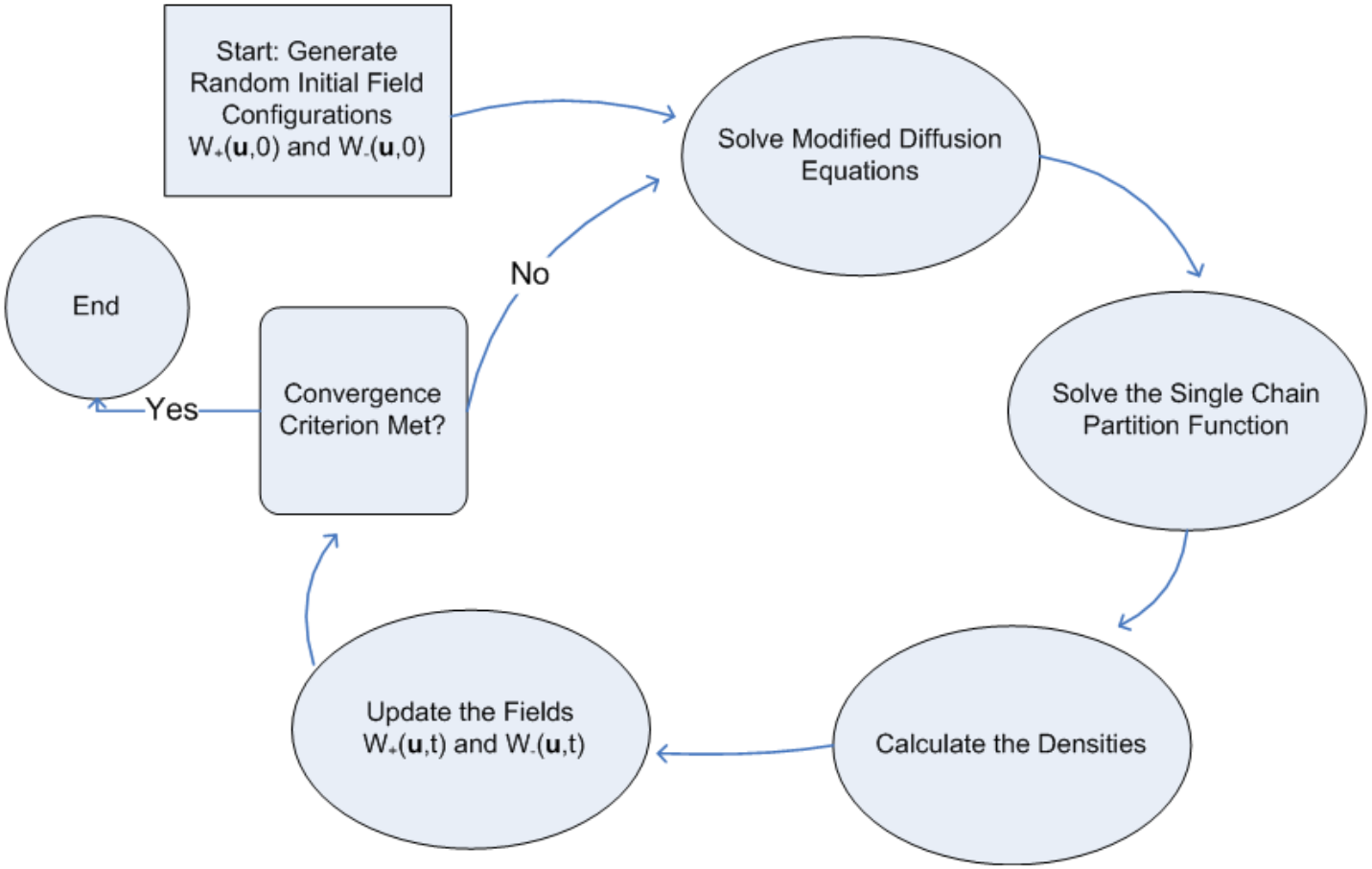

Existence of Solutions

- Dynamics equations: ODE in a Banach space.

$$\frac{dy}{dt} = F(y); \quad F : (L^p(V))^2 \to (L^p(V))^2, \quad p \geq \frac{3}{2}$$

  - F is Lipschitz: Follows from Kato-Rellich + semigroup estimates: $q(s) = e^{s(\Delta - \psi)} q_0$
  - F is in fact Fréchet differentiable:

$$q(s) = e^{s\Delta} q_0 - \int_0^s s^{(s-t)\Delta} \psi e^{t\Delta} q_0 \, dt + O(\|\psi\|^2)$$

  - Picard's theorem: (Local) Existence and Uniqueness.
  - Global existence: Extension of local solutions.

Phase separation: Bifurcation

- We consider symmetric solutions:

$$F(W,\Sigma,\chi_N)=0; \quad F:(L^p(V))^2\times(0,\infty)\to(L^p(V))^2, \quad p\geq\frac{3}{2}$$

- Homogeneous solution: $F(0,0,\chi_N)=0 \ \ \forall\chi_N$
- Fréchet derivative:

$$F'(0,0,\chi_N)=\begin{pmatrix} T_{11} & T_{12} \\ T_{21} & T_{22} \end{pmatrix},$$

where

$$\begin{aligned}
T_{11} &= 2\Delta^{-1}+2\Delta^{-2}\left(I-e^{\Delta}\right), \\
T_{12} &= 2(1-2f)\Delta^{-1}+2\Delta^{-2}\left(e^{f\Delta}-e^{(1-f)\Delta}\right), \\
T_{21} &= -T_{12}, \\
T_{22} &= -2\Delta^{-1}-2\Delta^{-2}\left(3I-2e^{f\Delta}-2e^{(1-f)\Delta}+e^{\Delta}\right)-\frac{2}{\chi_N}.
\end{aligned}$$

P. Von Soosten, *Senior Thesis at UCSB (2011)*

Phase separation: Bifurcation (cont.)

- Crandall-Rabinowitz-type of bifurcation.

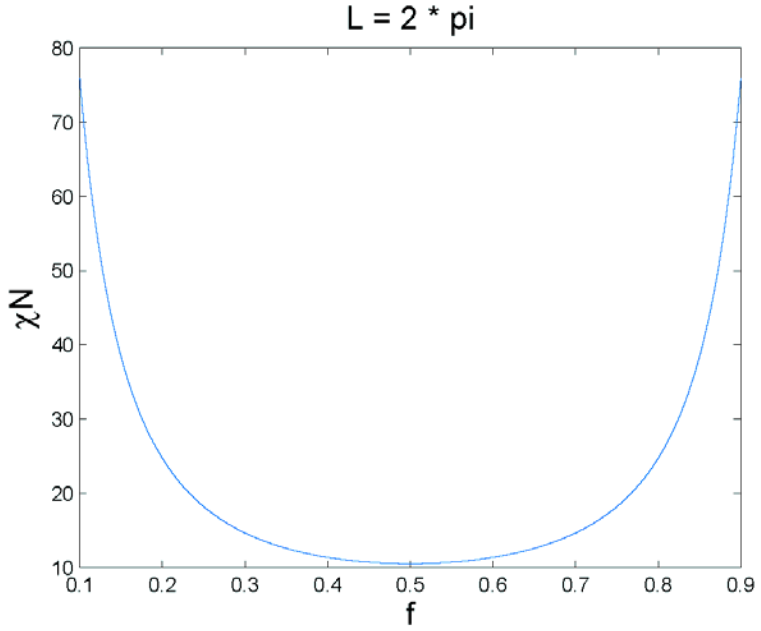

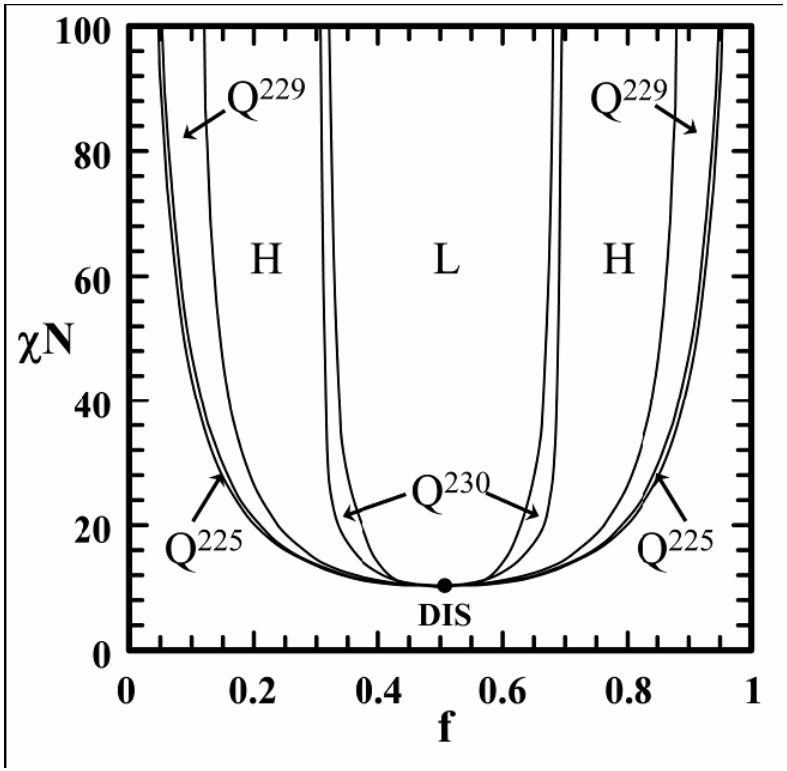

E.W. Cochran, CJGC, and G.H. Fredrickson, *Macromolecules, 39(7), (2006).*

SCFT Equations: Numerics

- Dynamics:
  - Mean field (saddle point) solution (SCFT)
  - Solving for Q and densities: most numerically expensive step.

$$
\begin{aligned}
\frac{\partial W}{\partial t} &= \phi_A(x;W,\Sigma) - \phi_B(x;W,\Sigma) + 1 - 2f - \frac{1}{\chi_N} W, \\
\frac{\partial \Sigma}{\partial t} &= \phi_A(x;W,\Sigma) + \phi_B(x;W,\Sigma) - 1, \\
\phi_A(x;W,\Sigma) &= \frac{1}{Q}\int_0^f q(x,s)q^\dagger(x,1-s)\,ds, \\
\phi_B(x;W,\Sigma) &= \frac{1}{Q}\int_f^1 q(x,s)q^\dagger(x,1-s)\,ds, \\
Q &= \frac{1}{V}\int_V q(x,1)\,dx.
\end{aligned}
$$

SCFT Equations: Challenges

- Main ingredients:
  - Time-stepping of the chemical potentials.
  - Solver for modified diffusion equation.
  - Integration along the polymer chain.
- Nonlinear, nonlocal equations.
- Fully implicit: too costly.
- Semi-Implicit Scheme via Linearization:

$$\frac{W^{n+1} - W^n}{\Delta t} = \mathcal{L}[W^{n+1}] + F[W^n] - \mathcal{L}[W^n]$$

Semi-Implicit Scheme for SCFT

- Consider: $\frac{\partial q}{\partial s} = \Delta q - \epsilon w q;$

- **Asymptotic expansion (RPA):**

$$\begin{aligned} q(x,s) &= 1 + \varepsilon \sum_{k \neq 0} \hat{q}_1(k,s) e^{ikx} + O(\varepsilon^2), \\ q^\dagger(x,s) &= 1 + \varepsilon \sum_{k \neq 0} \hat{q}_1^\dagger(k,s) e^{ikx} + O(\varepsilon^2). \end{aligned}$$

- **Leading term in the density:**

$$\begin{aligned} \phi_A(x) &= f + \varepsilon \sum_{k \neq 0} e^{ikx} \int_0^f (\hat{q}_1(k,s) + \hat{q}_1^\dagger(k,1-s))\, ds + O(\varepsilon^2), \\ \phi_B(x) &= 1 - f + \varepsilon \sum_{k \neq 0} e^{ikx} \int_f^1 (\hat{q}_1(k,s) + \hat{q}_1^\dagger(k,1-s))\, ds + O(\varepsilon^2). \end{aligned}$$

Semi-Implicit Scheme for SCFT

$$\begin{aligned}
\frac{\Sigma^{n+1}-\Sigma^{n}}{\Delta t} &= -(g_{AA}+2g_{AB}+g_{BB})*\Sigma^{n+1}+(\phi_A^n+\phi_B^n-1) \\
&\quad +(g_{AA}+2g_{AB}+g_{BB})*\Sigma^{n}, \\
\frac{W^{n+1}-W^{n}}{\Delta t} &= \phi_A^*-\phi_B^*+1-2f-\frac{2}{\chi N}W^{n+1}.
\end{aligned}$$

$$\begin{aligned}
\widehat{g}_{AA}(k) &= \frac{2}{|k|^4}\left(f|k|^2+e^{\ |k|^2 f}-1\right), \\
\widehat{g}_{AB}(k) &= \frac{1}{|k|^4}\left(1-e^{-|k|^2 f}\right)\left(1-e^{-|k|^2(1-f)}\right), \\
\widehat{g}_{BB}(k) &= \frac{2}{|k|^4}\left((1-f)|k|^2+e^{\ |k|^2(1-f)}-1\right).
\end{aligned}$$

This scheme is unconditionally stable.

H.D. Ceniceros and G.H. Fredrickson, *Multiscale Modeling and Simulation*, 2(3), 452-474, 2004

Modified Diffusion Equation

$$\begin{aligned} \frac{\partial q}{\partial s} &= \Delta q - \psi q, \quad x \in V, \quad s \in (0,1), \\ q(x,0) &= 1, \end{aligned}$$

Operator Splitting (2nd order):

$$q_{n+1} = e^{-\frac{\psi \Delta s}{2}} e^{\Delta s \Delta} e^{-\frac{\psi \Delta s}{2}} q_n$$

G. Strang, *Numerische Mathematik*, 6, 1964

K. O. Rasmussen and G. Kalosakas, *Journal of Polymer Science B: Polymer Physics*, 2002, 40, 1777

Solving the Modified Diffusion Equation

Modified Diffusion Equation: $\frac{\partial q}{\partial s} = \Delta q - \psi q$

Fourth Order BDF, initialized with Backward Euler + Extrapolation:

$$\begin{aligned}\frac{25}{12}q_{n+1} &= 4q_n - 3q_{n-1} + \frac{4}{3}q_{n-2} - \frac{1}{4}q_{n-3} + \Delta s[\Delta q_{n+1} \\ &\quad -w(u)(4q_n - 6q_{n-1} + 4q_{n-2} - q_{n-3})]\end{aligned}$$

Trapezoidal rule with endpoint corrections:

$$\int_I f\,ds = \Delta x \sum_{i=0}^{m}{}' f_i - \frac{\Delta s^2}{12}\left(\frac{3f_m - 4f_{m-1} + f_{m-2}}{2\Delta s} - \frac{3f_0 - 4f_1 + f_2}{2\Delta s}\right) + O(\Delta s^4)$$

E.W. Cochran, CJGC, and G.H. Fredrickson, *Macromolecules, 39(7), pp. 2449-2451 (2006)*

Stability of the gyroid phase

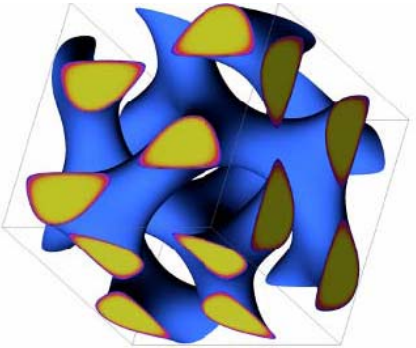

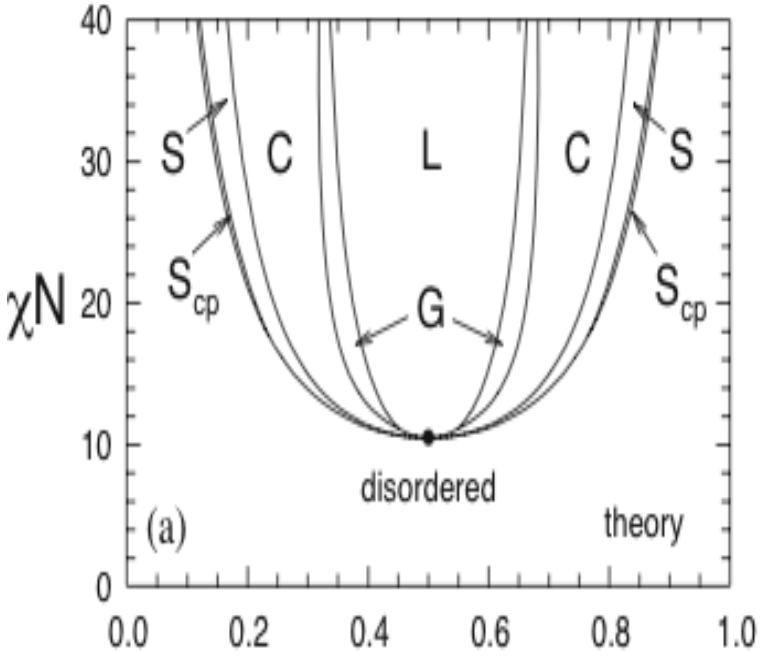

Matsen, M.W.; Schick, M.; *PRL*, 72(16) (1994).

Matsen, M. W.; Bates, F. S. *Macromolecules 29, (1996).*

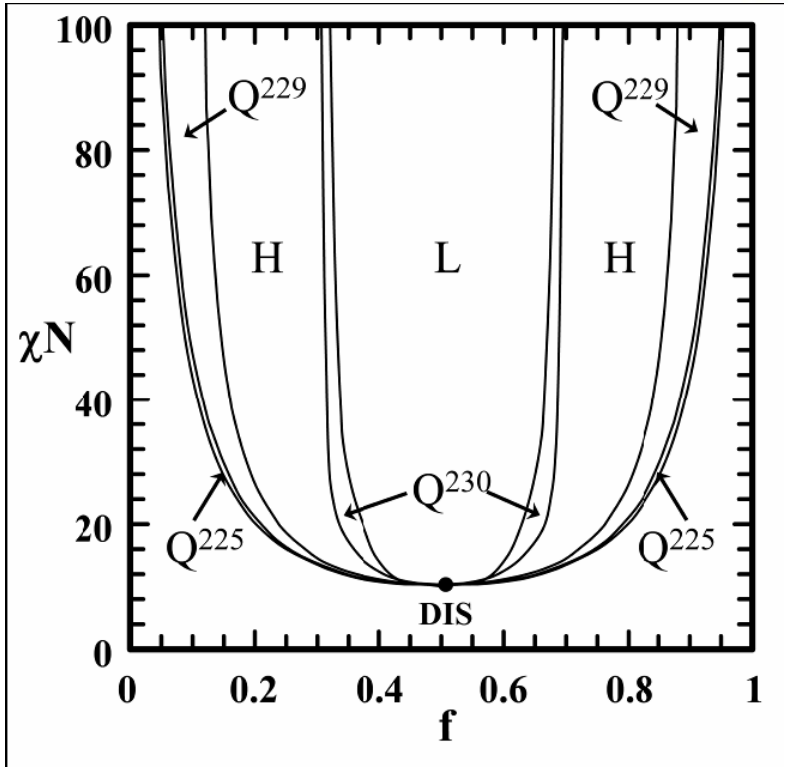

E.W. Cochran, CJGC, and G.H. Fredrickson, *Macromolecules, 39(7), (2006).*

Block-Copolymers on Curved Surfaces

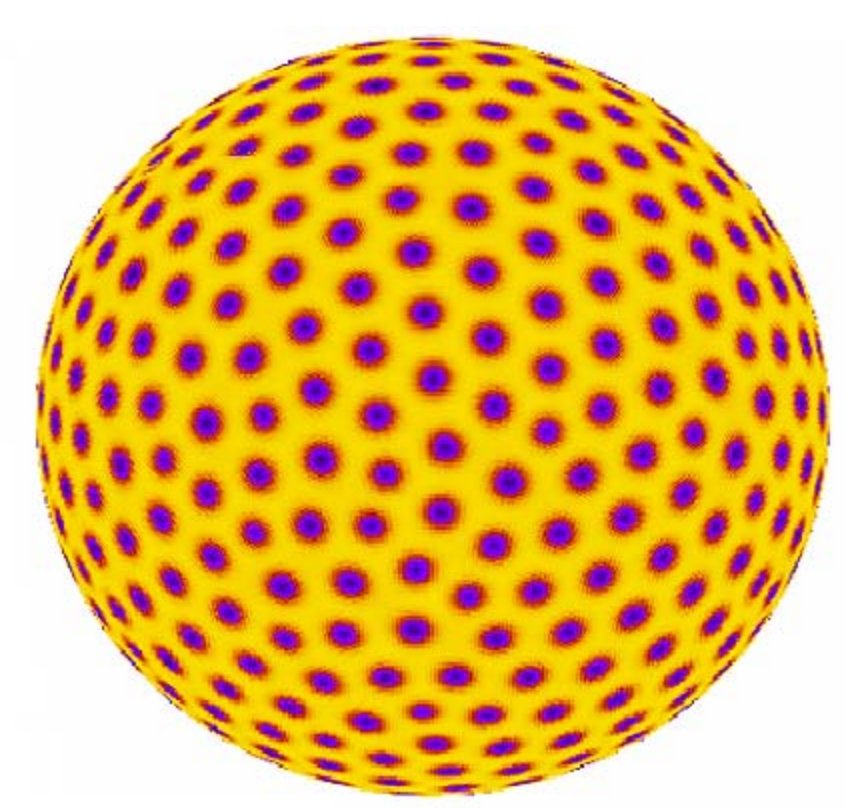

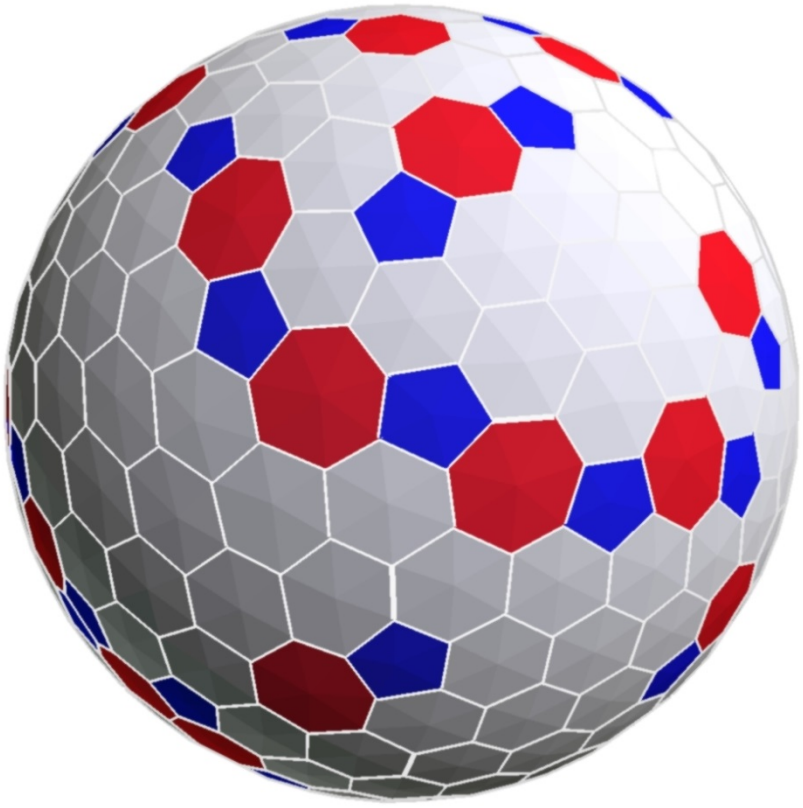

Total of 446 domains:
69 (5-fold) , 350 (6-fold) , and 57 (7-fold)

Lamellar phase

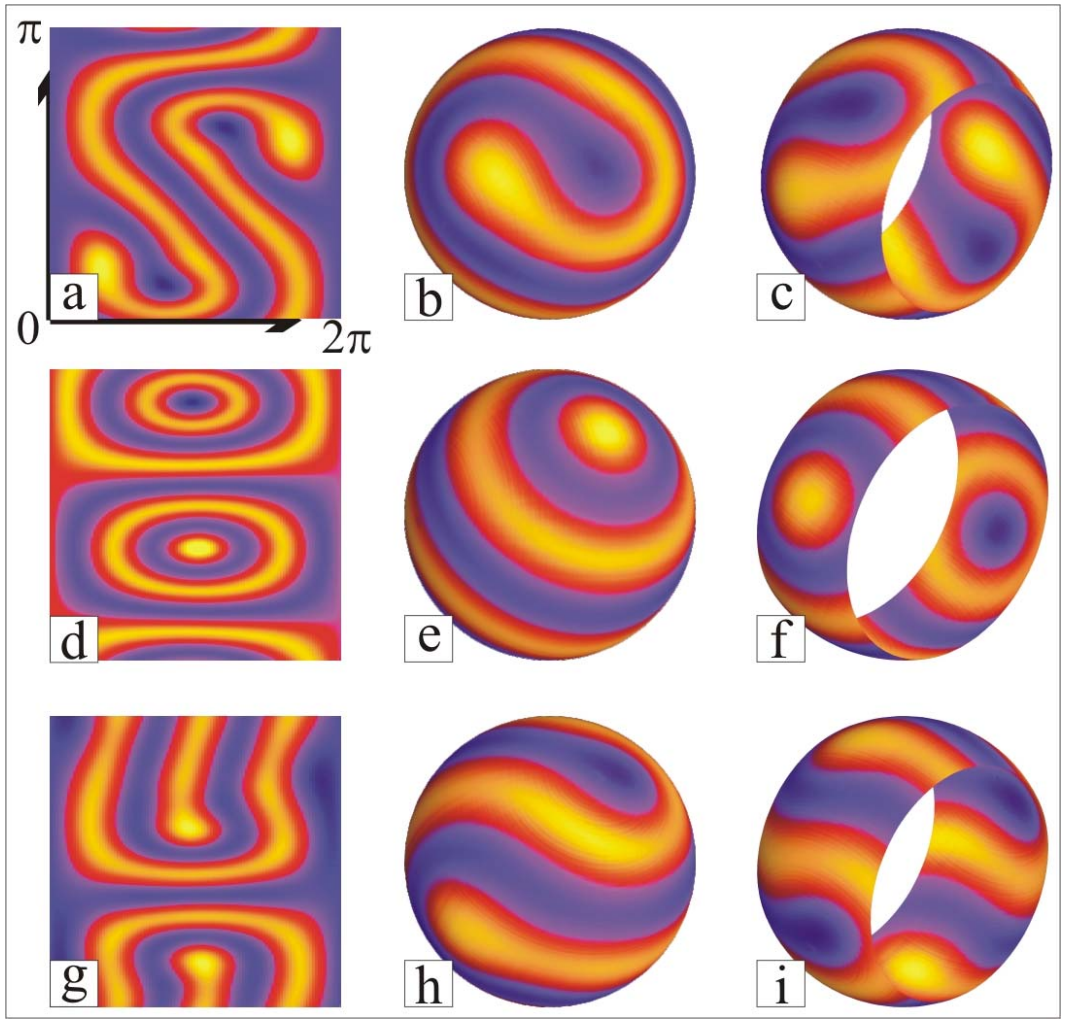

Spiral

Hedgehog

Quasibaseball

T.L. Chantawansri, A.W. Bosse, A. Hexemer, H.D. Ceniceros, C.J. García-Cervera, E.J. Kramer, and G.H. Fredrickson,
Phys. Rev. E, 75(3), 031802 (2007)

Lithography: AB in a Square Well

f_A = 0.7
B-cylinders in
hexagonal arrays
w/o confinement

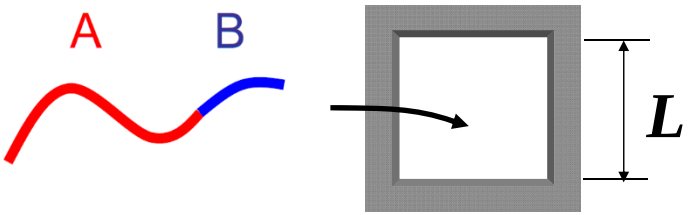

square arrays?

A-attractive square well
L = 14 R_g

Representative (normalized) density profiles of A-segment

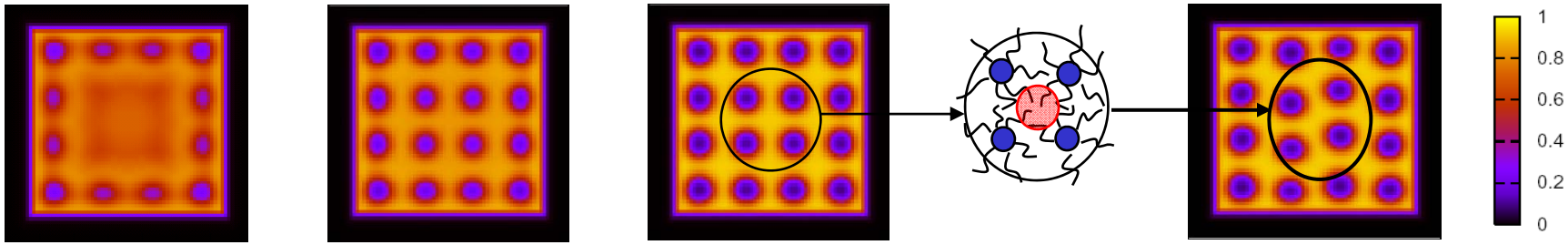

χN = 13.75 → 15.75 → 17

Tetragonal ordering is induced by the square lateral confinement during annealing stage.

17 →

Lattice subsequently twists into hexagonal ordering in order to reduce the stress in the interstitial sites.

S.-M. Hur, CJGC, E. Kramer, G.H. Fredrickson, *Macromolecules, 42(15), pp. 5861-5872 (2009);* S.-M. Hur, CJGC, G.H. Fredrickson, *submitted, (2011)*

AB + A in a Square Well

- A-homopolymer additive stabilizes tetragonal ordering

f_A = 0.7
B-cylinder forming diblock

α = 1.75 (N_{Ah}/N)
V_{Ah} = 0.23
A(major block)-homopolymer

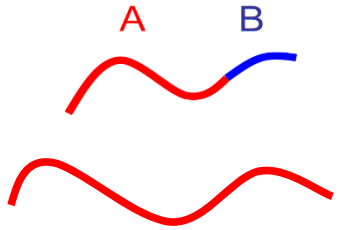

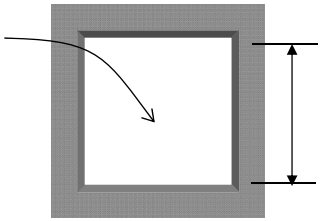

L = 23 R_g

B-attractive wall

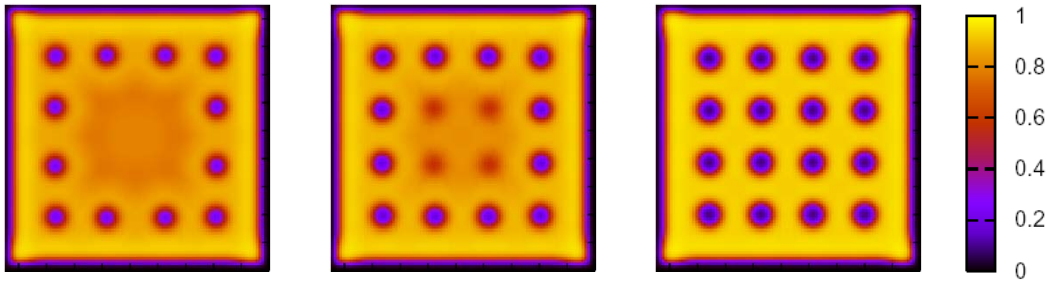

Evolution of total A-segment

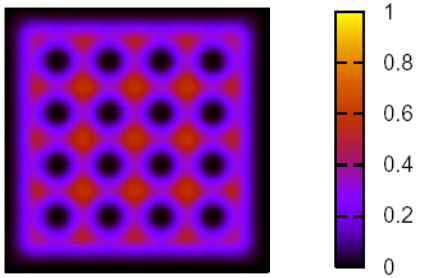

A-homopolymer segment concentration

A-homopolymer localization decreases the free energy of the square configuration such that it is energetically more favorable than the hexagonal configuration.

Bent Lines : AB + A + Confinement

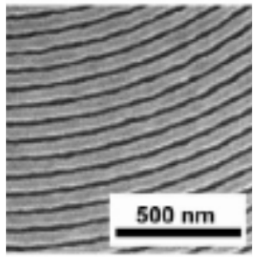

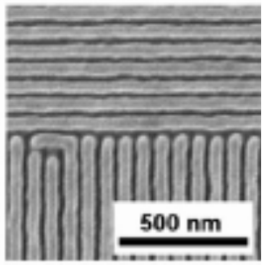

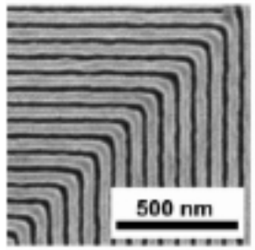

M. P.Stoykovich et al. *Materials Today*. 2006, 9(9), 20

f_A = 0.5, Channel Width = 9 R_g

AB + neutral wall

AB + A-attractive wall

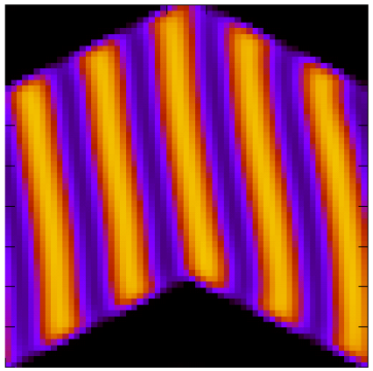

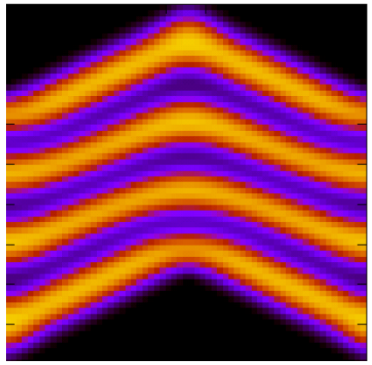

~ 12 .7R_g

+ A (α = 0.5 (N_{Ah}/N), V_{Ah}=0.2)

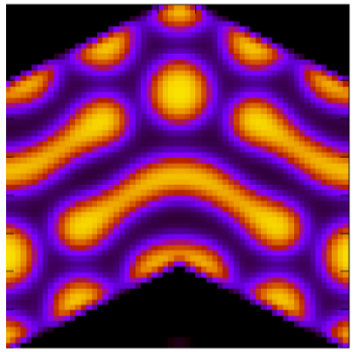

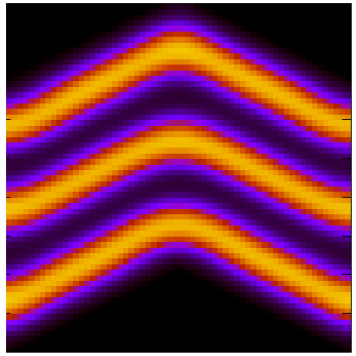

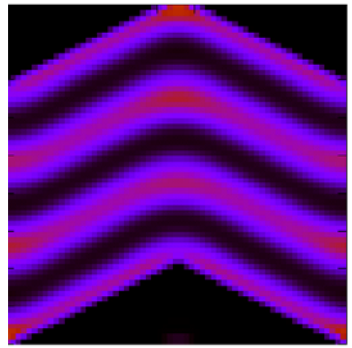

Dynamical Self-Consistent Field Theory

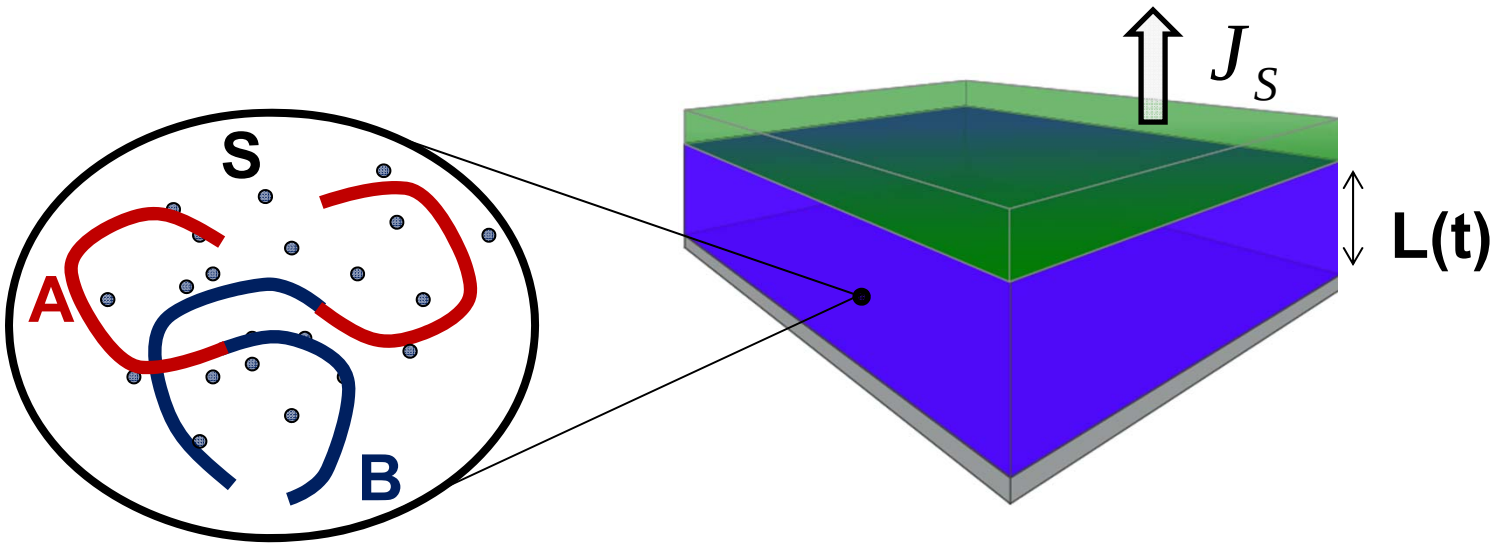

$$\partial_{\bar{t}}\phi_K = \nabla \cdot M_K \nabla \mu_K^{SCFT} + J_S \delta_{KS}$$

$$K = \{A, B, S\}$$

Density flux from SCFT free energy

Solvent removal from surface of film

S. Paradiso, K. Delaney, C.J. Garcia-Cervera, H.D. Ceniceros, G.H. Fredickson, *submitted*, 2013

SCFT Free Energy

Free energy $\Longrightarrow$ Legendre Transform of $H[w]$

$$F[\rho] = \sup_{w} \left\{ \int_V \rho w - H[w] \right\}$$

$$\Downarrow$$

$$\rho(\mathbf{x}) = \phi(\mathbf{x}; w^*) \quad (\text{Feynman} - \text{Kac})$$

Nonlinear, Nonlocal equation

Chemical Potential: SCFT Free Energy

$$\mu(r,t)_K^{SCFT} = \left.\frac{\delta H}{\delta \phi(r,t)_K}\right|_{w^*}$$

$$= C\left(\sum_J \chi_{KJ}\phi(r,t)_J - w(r,t)_K^* + \zeta\left(\left(\sum_J \phi(r,t)_J\right) - 1\right)\right)$$

$$\hat{\phi}_K(r;\underline{w}^*) = \int q(r,s;\underline{w}^*)q'(r,s;\underline{w}^*)ds = \phi_K(r,t)$$

Parameters Involved In Our Study

$\chi_{AB}\ \chi_{AS}\ \chi_{BS}$

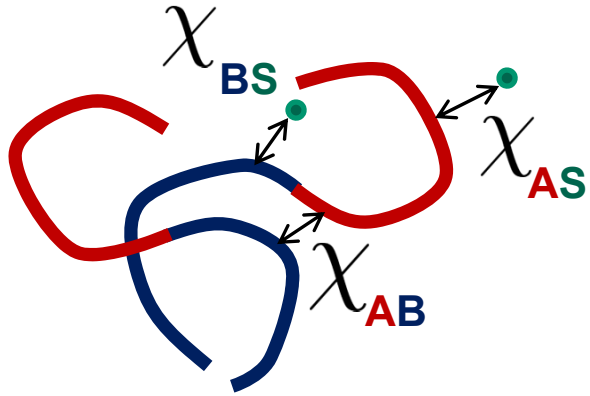

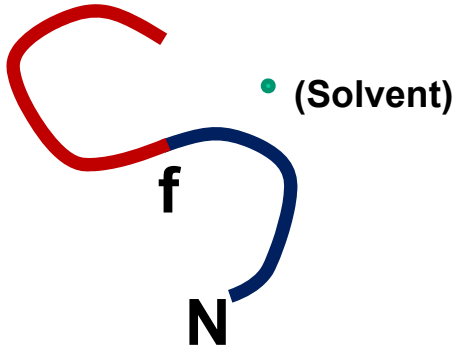

f, N

ϕ_S^{eq}

$\chi_{AB}^{\mathrm{eff}} N = (1-\phi_S^{\mathrm{eq}})\chi_{AB} N$

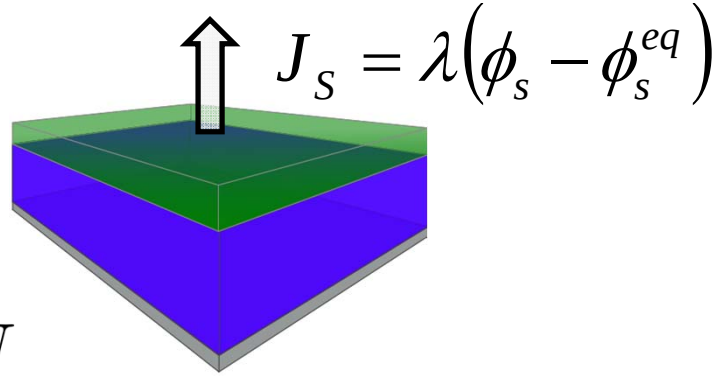

Moving Boundary Model

$$\partial_{\bar{t}}\phi_K = \nabla \cdot M_K \nabla \mu_K^{SCFT} + J_S \delta_{KS}$$

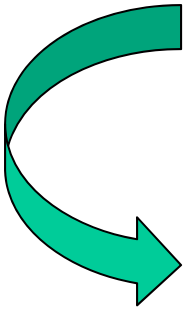

$$\bar{z} = \frac{z}{L(t)}$$

$$\left(\frac{\partial \phi}{\partial t}\right)_{\bar{z}} = \left(\frac{\partial \phi}{\partial t}\right)_z + \left(\frac{\partial \phi}{\partial z}\right)_t \left(\frac{\partial z}{\partial t}\right)_{\bar{z}}$$

$$= \nabla \cdot M \nabla \mu^{SCFT} + \bar{z} L'(t) \left(\frac{\partial \phi}{\partial z}\right)_t$$

Verification of Continuum Dynamics

MD Simulation Details:

- **6-12 LJ Fluid**
- **FENE bonds**
- **Strong 10-4 LJ interaction with z=0 surface prevents a 'floating' film**

Polymer →

Solvent →

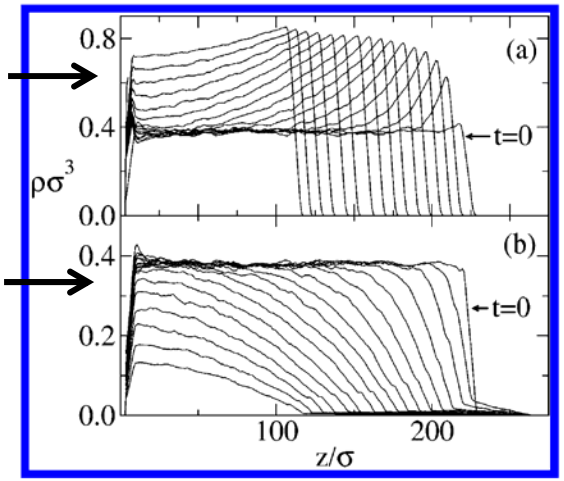

Typical Moving Boundary Model Profiles:

N=10
K=-1.0
XN_{Surf}=3.3

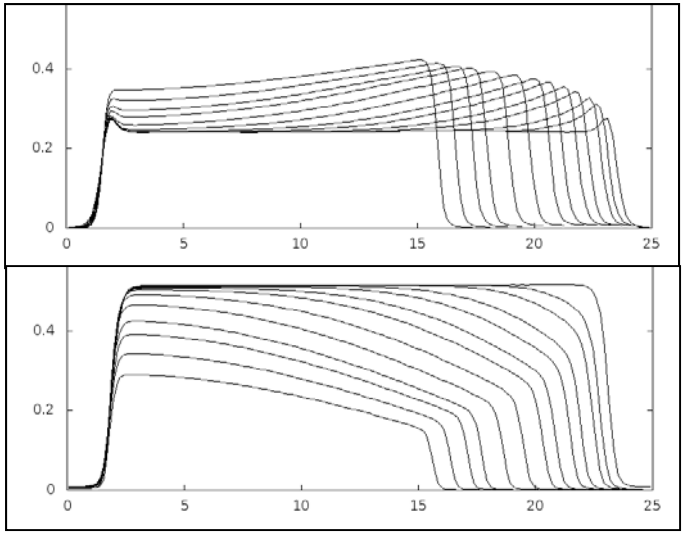

N=10
K=-7.0
XN_{Surf}=3.3

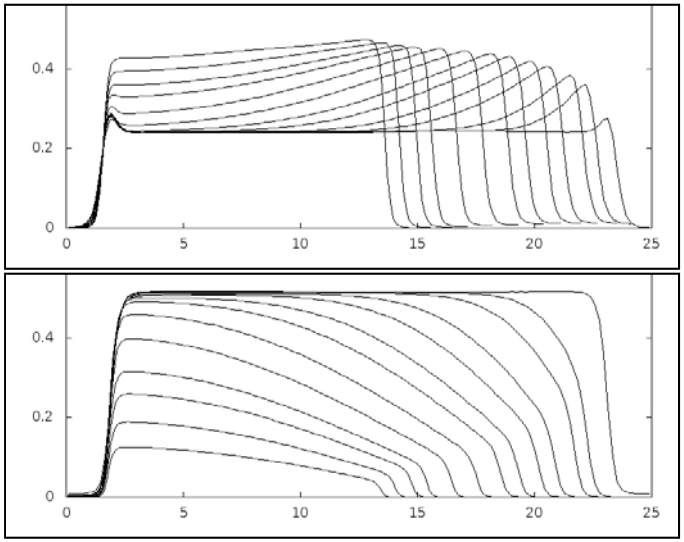

1. Tsige, M. Molecular dynamics study of the evaporation process in polymer films. *Macromolecules* 19, 1405 (2004).

Evaporation Dynamics in 2D: Lamellae

$$\chi_{AB}N = 22$$
$$f_{\mathrm{BCP}} = 0.5$$
$$\phi_S^{eq} = 0.3$$

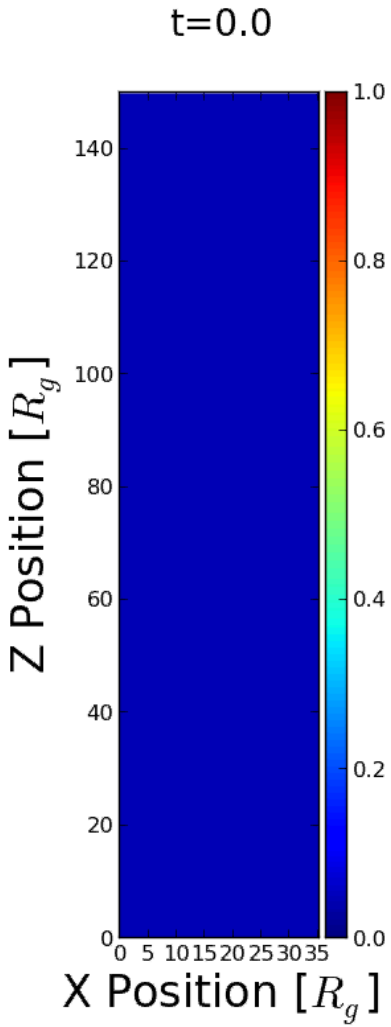

$$\chi_{AB}N = 22$$
$$f_{\mathrm{BCP}} = 0.5$$
$$\phi_S^{eq} = 0.18$$

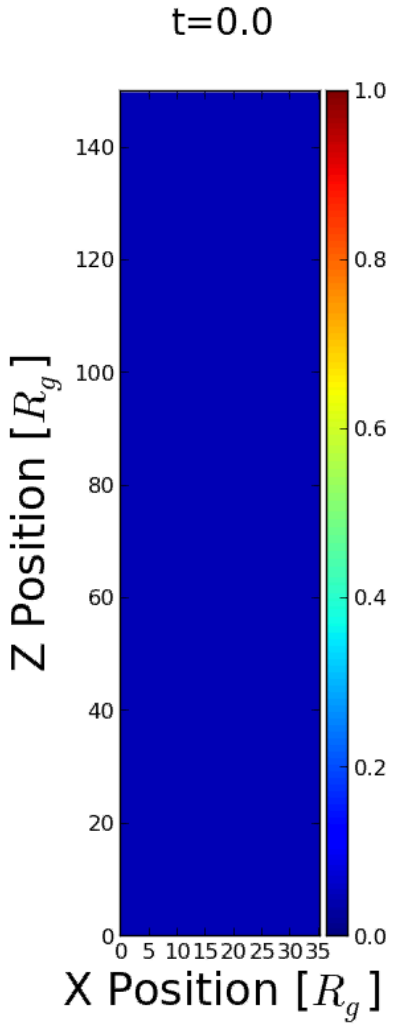

Morphology Guided by Secondary Patterns

- Ordered phase **induces density correlations** in near-critical fluid beneath it.
  - **Every** dynamical result exhibits some form of this pattern

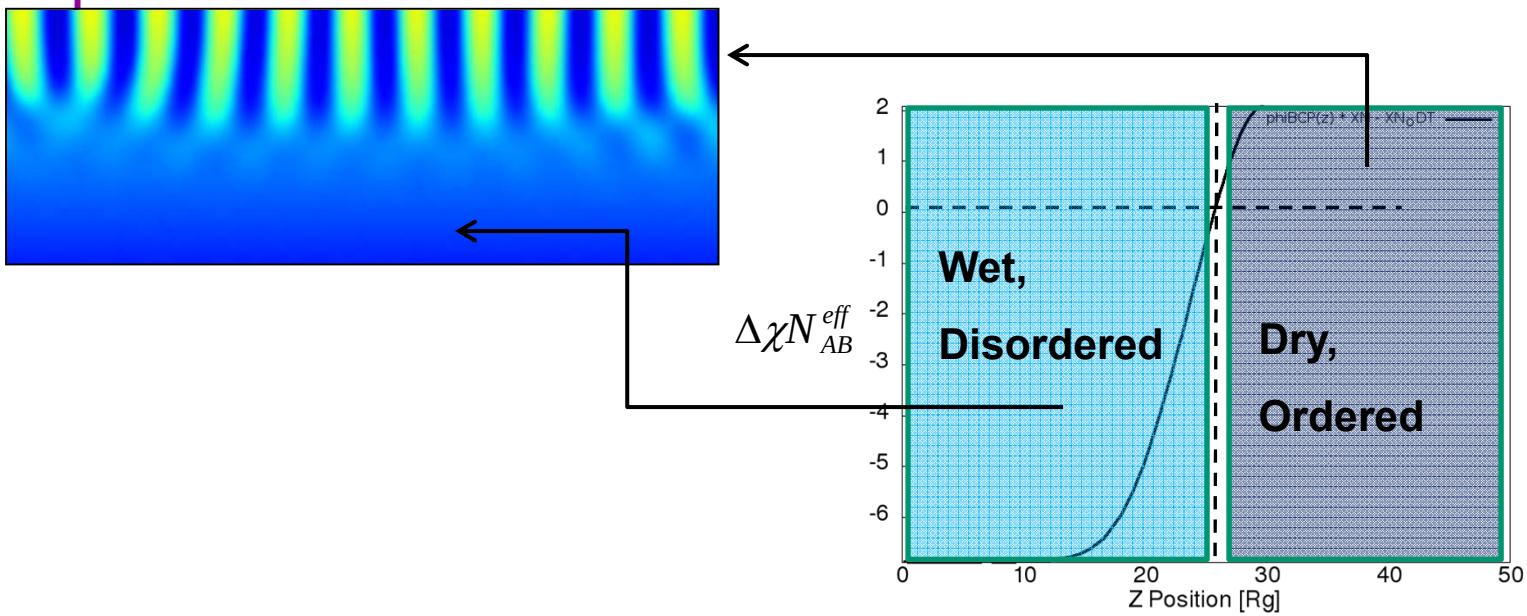

Molecular Origin of Induced Patterns

- Block connectivity
  - Stripes terminate in dangling chain ends of the **opposite type**
  - Results in an increase in the **probability of finding B segments** beneath **A-rich Lamellae**

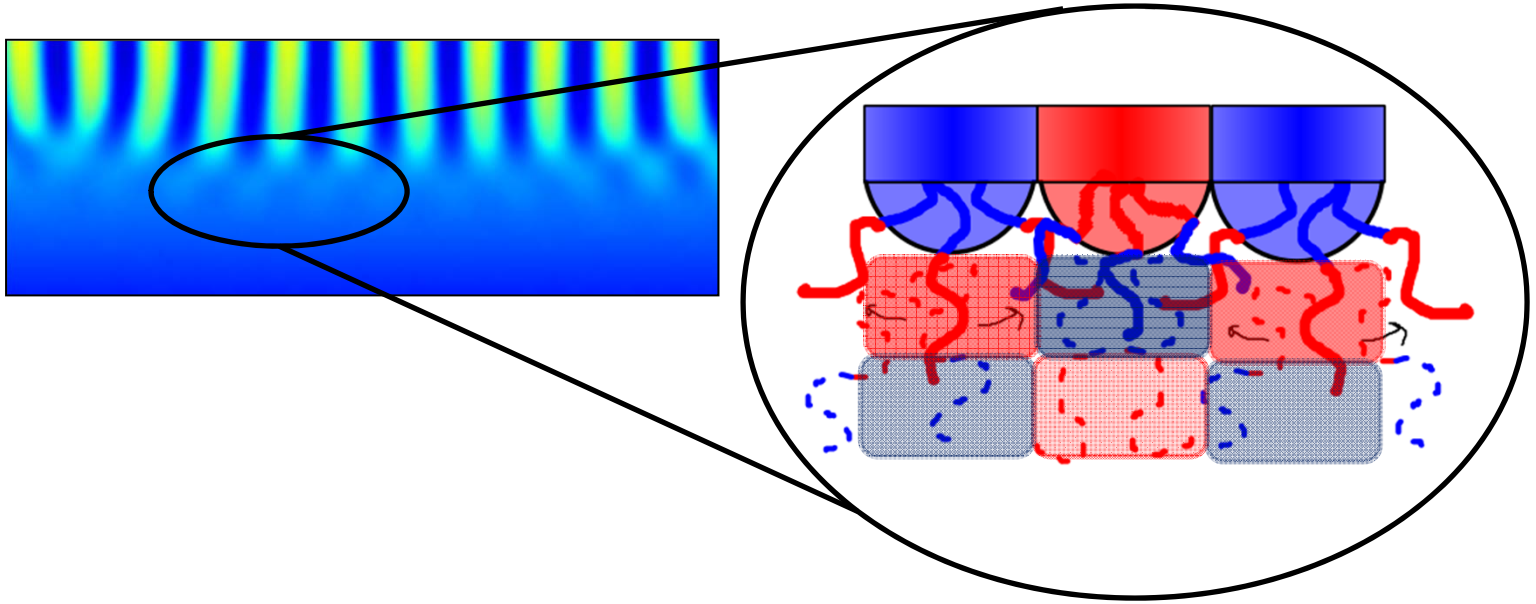

Control Experiments

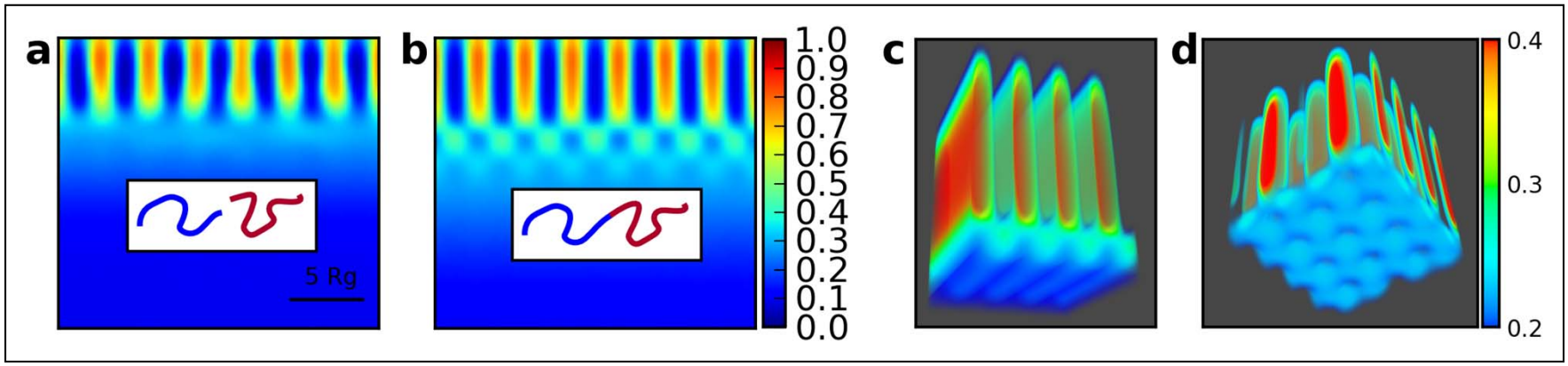

Evaporation simulations on a symmetric blend (a) and diblock (b) system implicate chain connectivity in patterning at the front.

Cylinder-forming systems (d) emerge a pattern analogous to the "struts" in (b) and (c)

Evaporation Trajectories

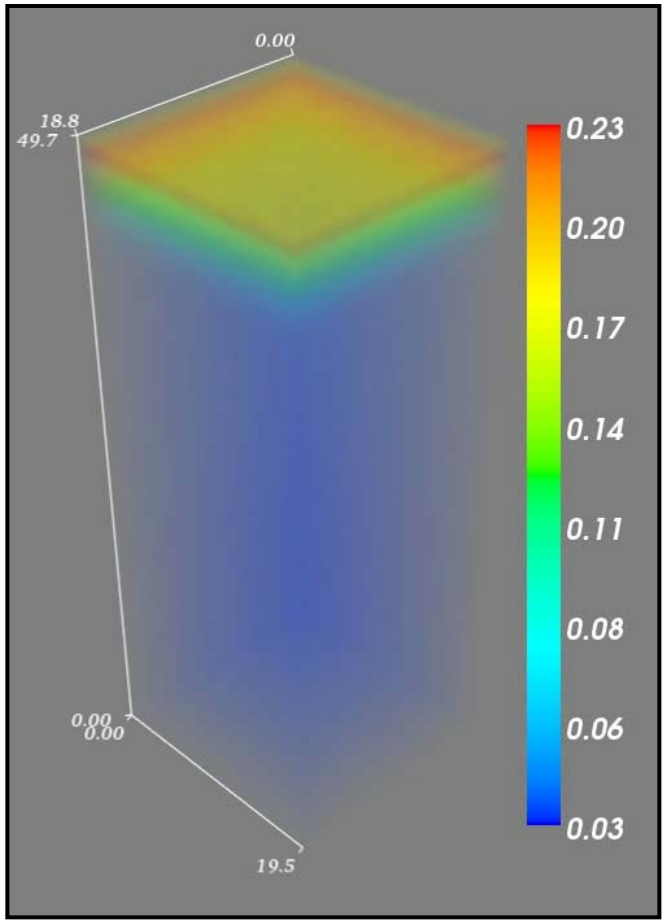

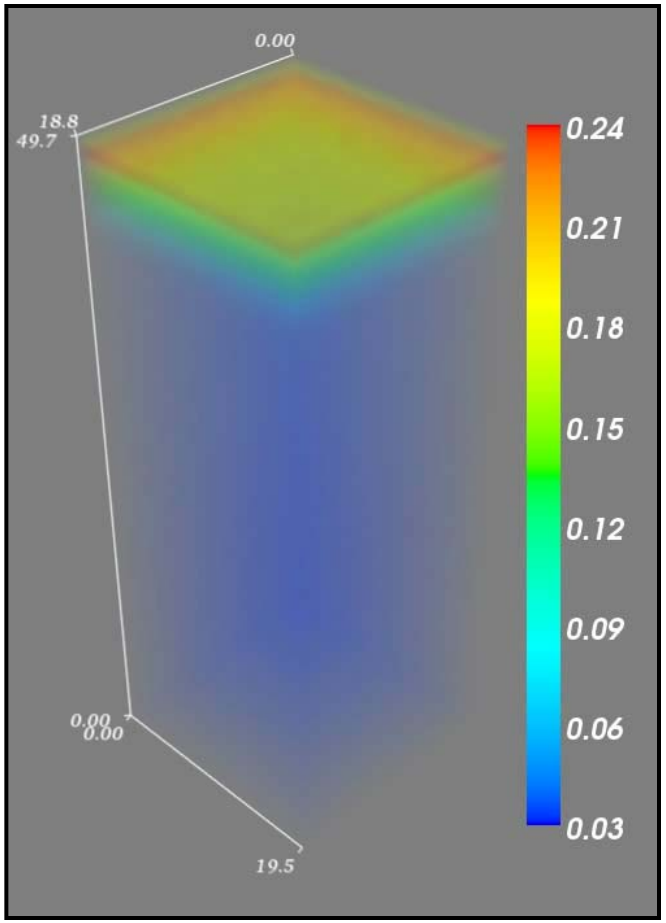

Trends in Surface Morphology

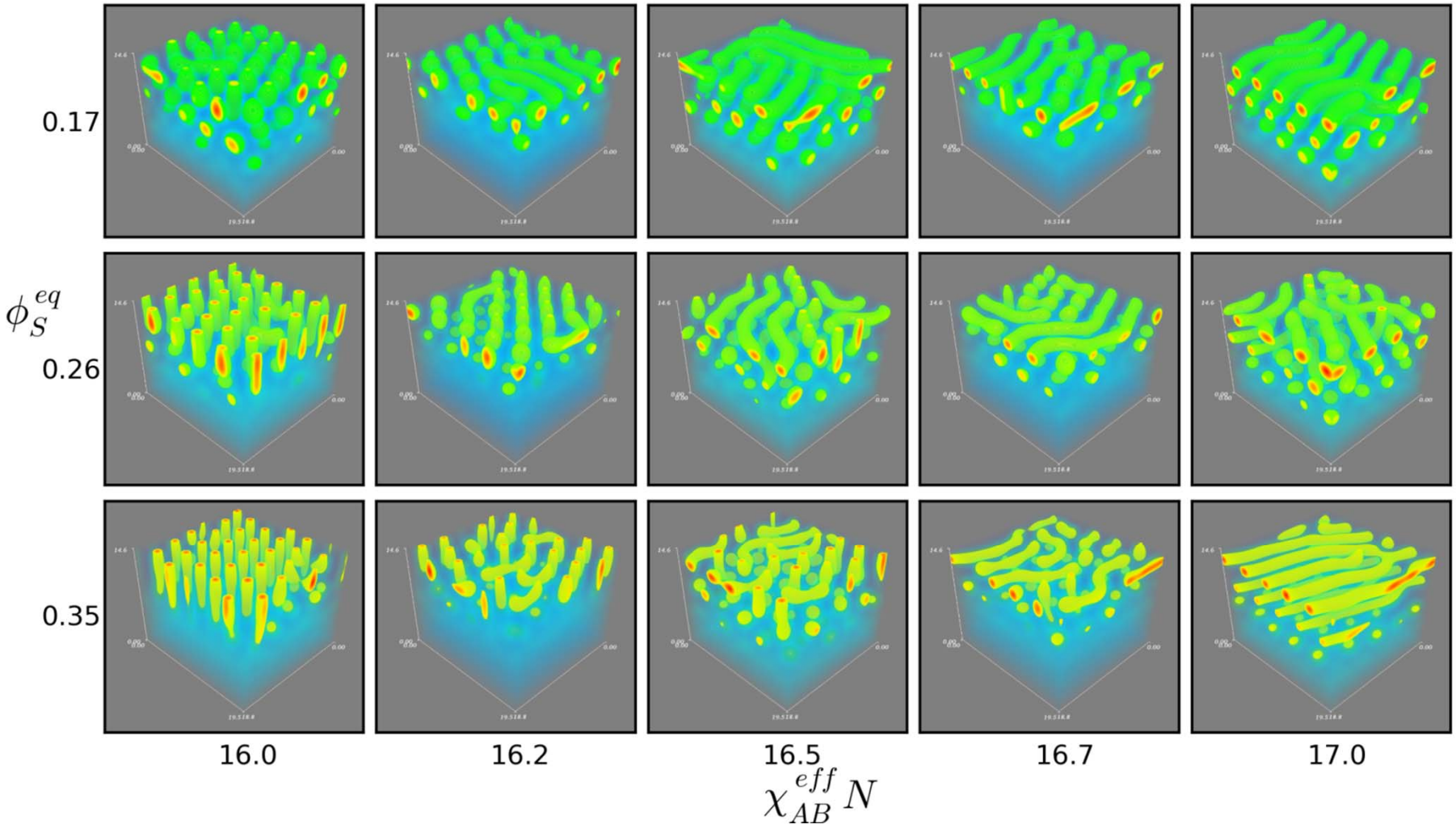

Trends in Surface Morphology

- Parameters ϕ_S^{eq} and χ_{AB}^{eff} are changed independently.
- χ_{AB}^{eff} increased: morphologies transition from perpendicular to horizontal.
- Changes in evaporation rate have minor effect.

Evaporation-driven Ordering

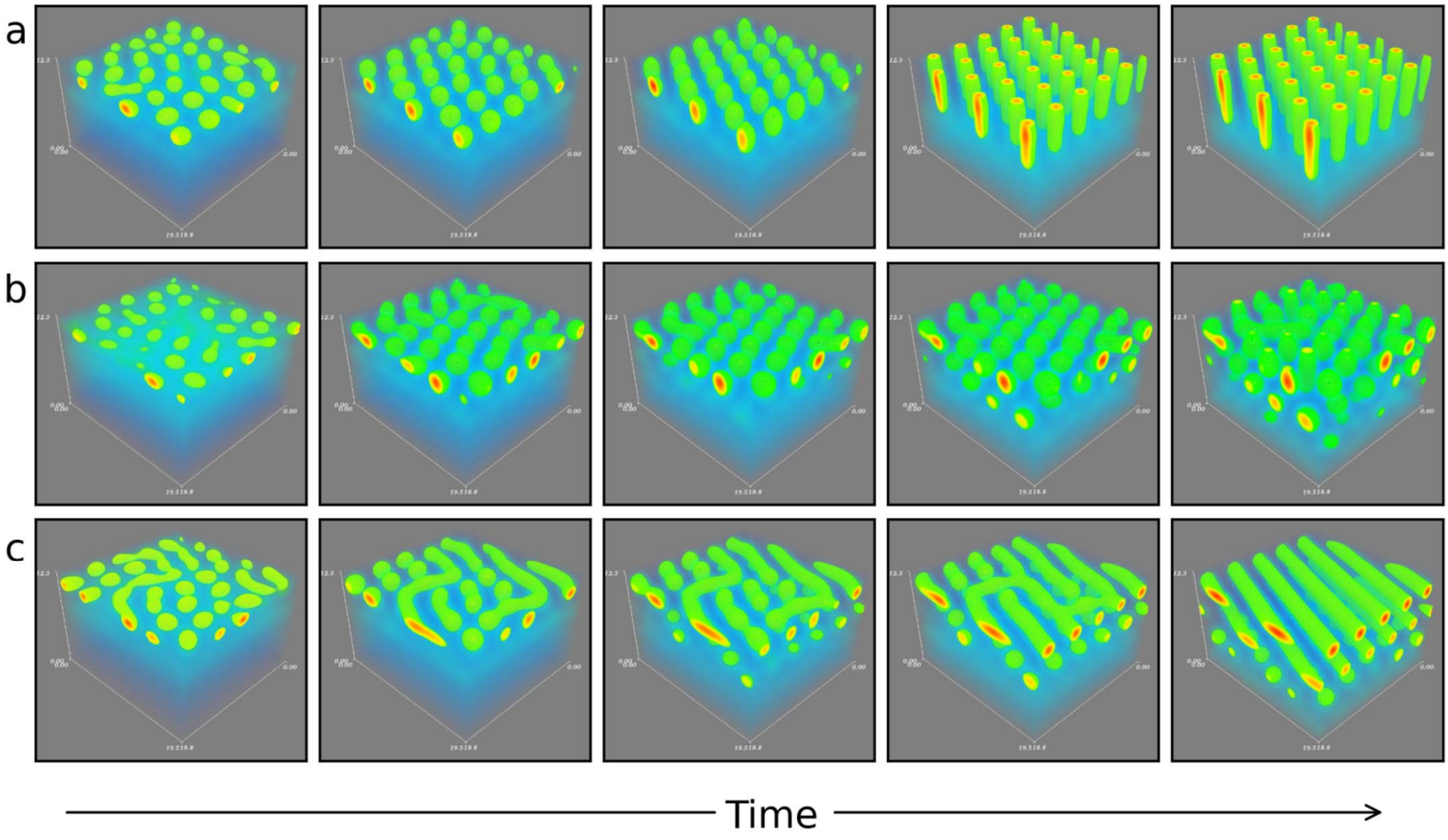

Evaporation-driven Ordering

- No order observed until unstable region near the surface forms: A layer of spheres appears.
- Spheres organize into a hexagonal lattice.
- A bifurcation occurs: For high χ_{AB}^{eff} , spheres are unstable as seen in phase diagram.
- Lower values of χ_{AB}^{eff} or slower evaporation rates provide sufficient time for solvent gradients to advance, and spheres to stretch.

Molecular Origin of Induced Patterns

- Block connectivity
  - Stripes terminate in dangling chain ends of the **opposite type**
  - Results in an increase in the **probability of finding B segments** beneath **A-rich Lamellae**

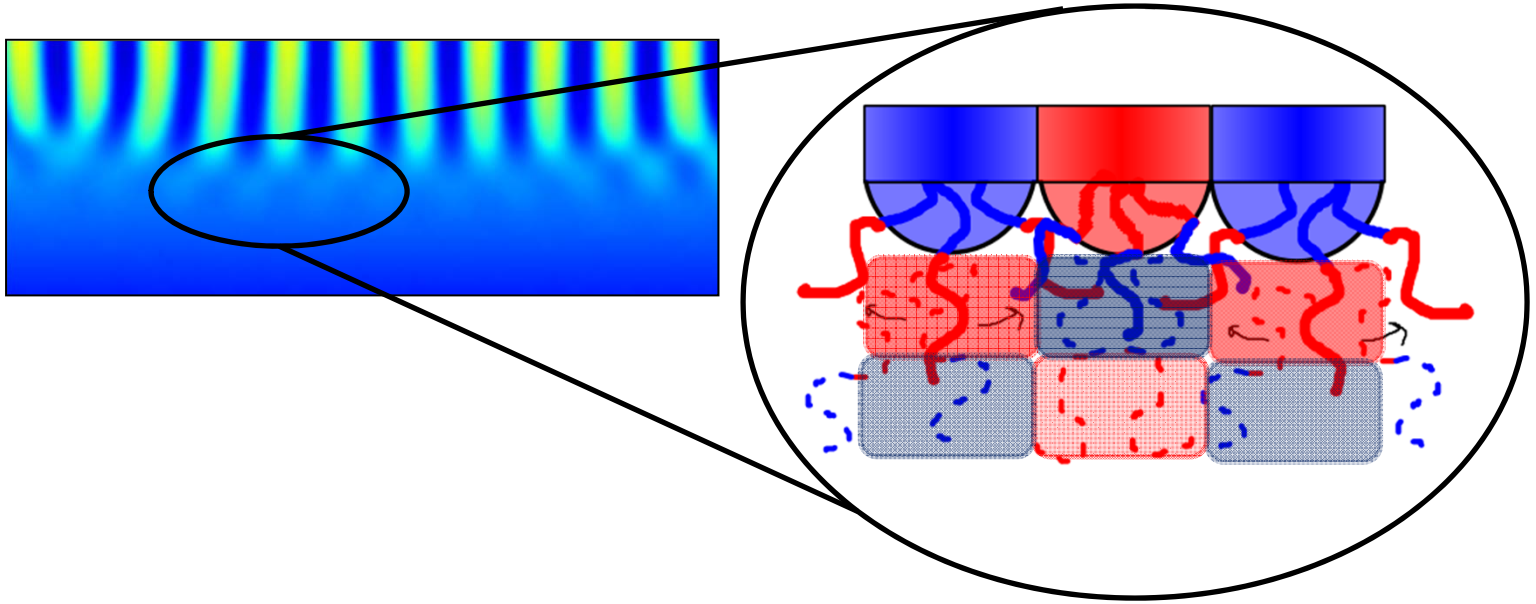

Mitigating the Correlation-Hole

- The correlation-hole pattern that forms beneath $\mathrm{C}_{\perp}$ presents an increased density of minority-block segments.

- Hypothesis: solvent selective for majority block will provide a barrier to forming this pattern and stabilize $\mathrm{C}_{\perp}$ fronts

Selective Solvent Results

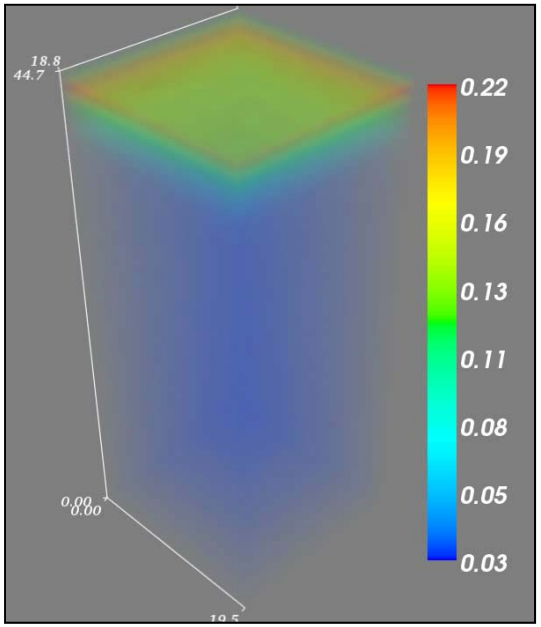

Minority-Selective

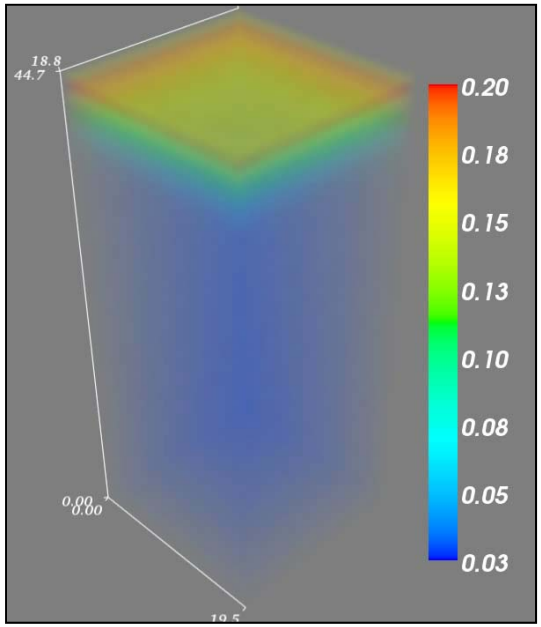

Neutral

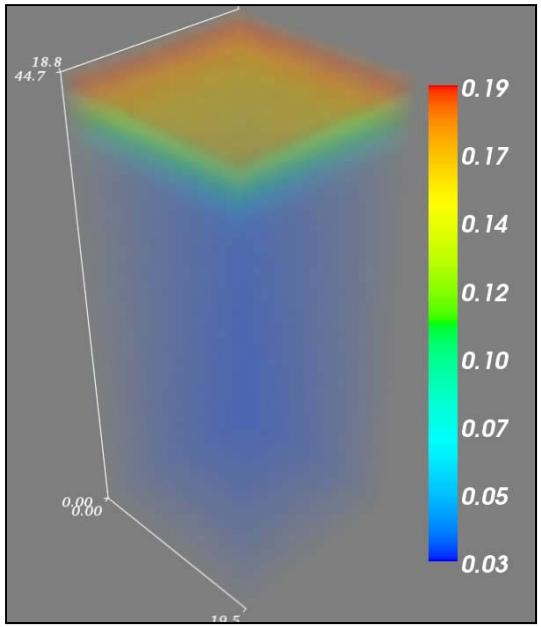

Majority-Selective

Selective Solvent Stabilizes Cylinder Formation

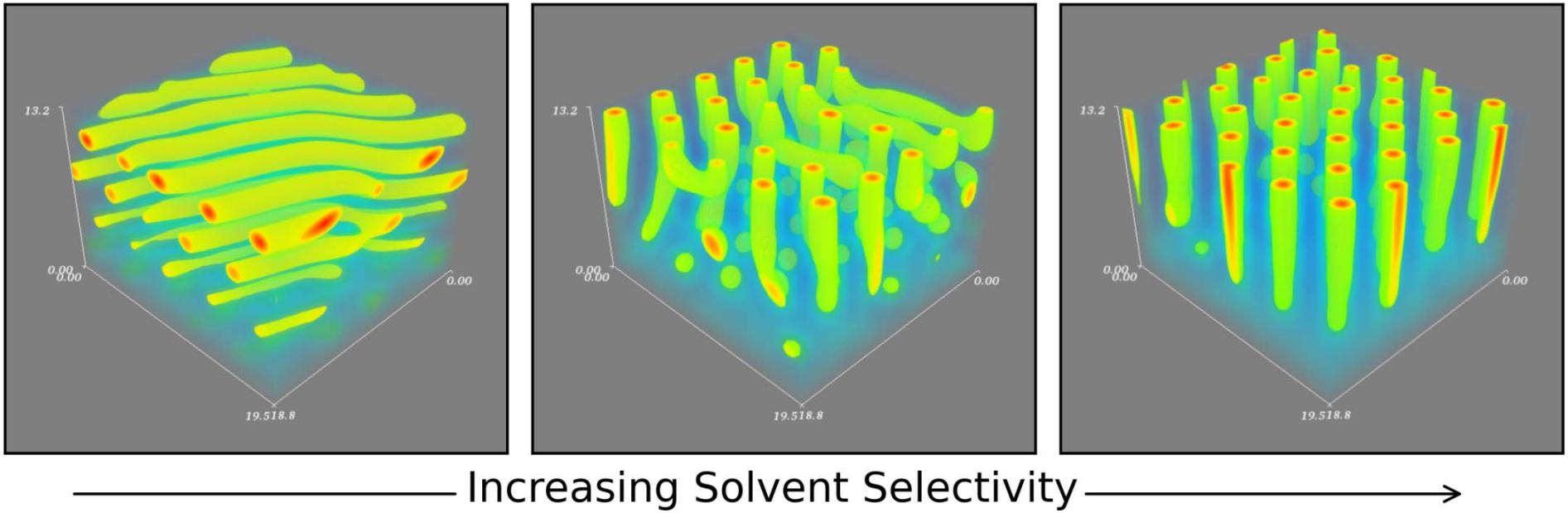

Overview and Future Work

- Developed efficient predictive numerical methodologies.
- Numerical experiments guide design of lithographic approaches and elucidate evaporation-induced pattern selection

- Further understanding of evaporation processes needed.
- Hydrodynamics: Coupling to Navier-Stokes?.
- Dynamic density functional theory: Can we invert the density? $\rho_0 = \rho(x; W, \Sigma) \rightarrow \text{Can we recover } W \text{ and } \Sigma?$
- Framework too complicated: Can we obtain reduced models?

*C.B. Muratov, M. Novaga, G. Orlandi, and CJGC in *"Singularities in nonlinear evolution phenomena and applications", CRM Series, 9, Birkhauser, (2009)*.

Acknowledgments

- We received partial support from the MARCO Center on Functional Engineered Nano Architectonics (FENA).
- This work made use of MRL Central Facilities supported by the MRSEC and MRI-R2 Programs of the National Science Foundation under award No. DMR05-20415 and NSF MRI-R2 0960316.
- Support provided by NSF CAREER, and NSF SOLAR awards.